



ELSEVIER

J. Non-Newtonian Fluid Mech. xxx (2006) xxx–xxx

**Journal of
Non-Newtonian
Fluid
Mechanics**

www.elsevier.com/locate/jnnfm

Four-field Galerkin/least-squares formulation for viscoelastic fluids

Oscar M. Coronado^a, Dhruv Arora^a, Marek Behr^{a,b,*}, Matteo Pasquali^{a,*}

^a Department of Chemical and Biomolecular Engineering and Computer and Information Technology Institute, Rice University, MS 362, 6100 Main Street, Houston, TX 77005, USA

^b Chair for Computational Analysis of Technical Systems, CCES, RWTH Aachen University, 52056 Aachen, Germany

Received 4 November 2005; received in revised form 14 February 2006; accepted 24 March 2006

Abstract

A new Galerkin/Least-Squares (GLS) stabilized finite element method is presented for computing viscoelastic flows of complex fluids described by the conformation tensor; it extends the well-established GLS method for computing flows of incompressible Newtonian fluids. GLS methods are attractive for large-scale computations because they yield linear systems that can be solved easily with iterative solvers (e.g., the Generalized Minimum Residual method) and because they allow simple combinations of interpolation functions that can be conveniently and efficiently implemented on modern distributed-memory cache-based clusters.

Like other state-of-the-art methods for computing viscoelastic flows (e.g., DEVSS-TG/SUPG), the new GLS method introduces a separate variable to represent the velocity gradient; with the aid of this variable, the conservation equations of mass, momentum, conformation, and the definition of velocity gradient are converted into a set of first-order partial differential equations in four unknown fields—pressure, velocity, conformation, and velocity gradient. The unknown fields are represented by low-order (continuous piecewise linear or bilinear) finite element basis functions.

The method is applied to the Oldroyd-B constitutive equation and is tested in two benchmark problems—flow in a planar channel and flow past a cylinder in a channel. Results show that (1) the mesh-convergence rate of GLS is comparable to the DEVSS-TG/SUPG method; (2) the LS stabilization permits using equal-order basis functions for all fields; (3) GLS handles effectively the advective terms in the evolution equation of the conformation tensor; and (4) GLS yields accurate results at lower computational costs than DEVSS-type methods.

© 2006 Elsevier B.V. All rights reserved.

Keywords: Stabilized finite element method; Viscoelastic flow; Galerkin/least-squares; Oldroyd-B fluid; Flow past a cylinder in a channel

1. Introduction

In the past decades, extensive research has been done on flows of liquids with micro–macro structure (also known as complex fluids); these fluids are found in several industrial and biological applications, e.g., polymer processing, coating of polymer solutions, ink-jet printing, microfluidic devices, and human as well as artificial organs (blood, synovial fluid). Usually these liquids display a viscosity dependent on the rate of straining and the flow kinematics (shear versus extension); they also show elasticity on time scales that overlap with the flow time scales.

Realistic models of flowing complex fluids are crucial for understanding and optimizing flow processes. Two main classes

of models have been proposed for modeling complex fluids: fine-grained models [1,2], (e.g., bead-spring or bead-rod models of polymer solutions), where the microstructure is represented by micromechanical objects governed by stochastic differential equations, and coarse-grained ones, where the microstructure is modeled by means of one or more continuum variables representing the expectation value of microscopic features (e.g., the conformation tensor in models of polymer solutions) [3–6]. Fine-grained models incorporate a richer degree of molecular details, but are still limited to fairly simple flows because of computational cost [7–9].

Coarse-grained models represent the liquid microstructure in terms of one or more conformation tensors; currently, these models are considered the most appropriate for large-scale simulation of complex flows of complex fluids. Typically, the conformation tensor obeys a hyperbolic partial differential transport equation. In polymer solutions and melts, this tensor represents the local expectation value of the polymer stretch and orientation, e.g., gyration or birefringence tensor. The elastic part

* Corresponding authors. Tel.: +1 713 348 5830; fax: +1 713 348 5478.

E-mail address: mp@rice.edu (M. Pasquali), behr@cats.rwth-aachen.de (M. Behr).

of the stress is related to the conformation tensor through an algebraic equation [3–6]. Such models include most “classical” rate-type stress-based differential models (e.g., Oldroyd-B, PTT, Giesekus, etc.) [3–6].

Simulations of complex flows of complex fluids require solving simultaneously the hyperbolic transport equation of conformation (or rate-type equation for the stress) together with the momentum and mass conservation equations; this poses several numerical challenges. In particular, obtaining mesh-converged solutions in simple benchmark flows at high Weissenberg number (Wi , the product of characteristic strain rate and fluid relaxation time) is still considered an open problem.

The Galerkin method is perhaps the most effective method for flows with free surfaces and deformable boundaries. However, the Galerkin method is unstable in advection-dominated problems, and yields spurious oscillations in the variable fields. Alternative methods have been developed to handle advection-dominated as well as purely hyperbolic equations—e.g., Streamline upwind/Petrov–Galerkin (SUPG) for high Reynolds number Newtonian flows [10] and viscoelastic flows [11], also Discontinuous Galerkin (DG) for viscoelastic flows [12].

When the Galerkin (or SUPG) method is applied to coupled partial differential equations, the selection of the interpolating functions for the various unknowns can be restricted by compatibility conditions—e.g., the Babuška-Brezzi condition in flows of incompressible Newtonian fluids [13,14]. Some compatibility conditions between the basis functions of velocity, pressure, velocity gradient, and conformation (or stress) must still be satisfied [15,16] by current Galerkin-type methods for simulating viscoelastic flows—e.g., the state-of-the-art DEVSS-TG/SUPG, which evolved from successive modifications of the EVSS method [17–22] (see also reviews by Baaijens [23] and Owens and Phillips [24]).

These two key hurdles (handling advection-dominated problem and satisfying compatibility conditions) have been overcome in Newtonian flows by using Galerkin/Least-Squares (GLS) methods [25–27]. Work on GLS methods applied to Newtonian flows has shown that Streamline-upwind terms appear naturally in the GLS form, that equal-order basis functions can be used for all fields (because the Least-Squares (LS) terms remove the compatibility condition), and that the resulting nonlinear algebraic equations yield a Jacobian matrix that can be solved more easily with preconditioned Generalized Minimum Residual method (GMRES) (because the LS terms yield a positive-definite Jacobian component). Moreover, using equal-order basis functions for all fields allows “nodal” (rather than “elemental”) accounting, which speeds up greatly matrix operations on distributed memory parallel machines [28].

Weakly consistent forms of GLS method have been applied to viscoelastic flows. Behr [25] introduced a three-field (velocity–pressure–elastic stress) GLS method and studied the flow of an Oldroyd-B liquid in a 4-to-1 contraction. However, a detailed comparison between this method and other published results was not performed, and the effect of the expression of the LS stabilization coefficient for the constitutive equation was not exam-

ined. This method has been refined and extended more recently to improve consistency by recovery of the velocity gradient as well as a more appropriate expression of the LS stabilization coefficient [29].

Fan et al. [30] independently introduced an incomplete GLS method for viscoelastic flow and tested its performance in a flow between eccentric cylinders, flow around a sphere in a pipe, and flow around a cylinder in a channel. This method did not include terms due to the LS form of the momentum equation (because it degraded performance) and of the constitutive equation; therefore, the method of Fan et al. [30] is better characterized as a pressure-stabilized SUPG method—see [31] for a description of pressure-stabilized methods for incompressible Newtonian flows.

This article presents a complete GLS method for computing flows of incompressible viscoelastic liquids modeled by conformation tensor or rate-type equations. The flow equations are converted to a set of four first-order partial differential equations by representing explicitly the velocity gradient tensor (as in DEVSS-G). The GLS weighted residual equations include naturally the consistent streamline upwinding for the advective terms in the conformation evolution equation (and in the momentum equation, although the presentation below is restricted to inertialess flows). The choice of basis functions for the four unknown fields (velocity, pressure, velocity gradient, and conformation) is not restricted by compatibility conditions; here, the unknown fields are represented by the simplest possible finite element basis functions—continuous piecewise bilinear on quadrilateral elements. The method is termed GLS4 to distinguish it from the previous GLS3 [25,29] method, in which the velocity gradient was not represented explicitly. The accuracy and stability of the method is demonstrated by using two benchmark problems—the flow in a planar channel and the flow past a cylinder in a channel—for an Oldroyd-B fluid.

It is worth noting that recent work [32–34] identified another source of instability in low-order finite difference and finite element methods for computing viscoelastic flows—namely, the inability of low-order methods to capture exponentially growing profiles of conformation or elastic stress in regions of strong flow. Such instability can be avoided by using the logarithm of the conformation tensor as field variable [32], which has the additional benefit of ensuring that the conformation tensor is automatically positive definite everywhere in the flow. The proposed GLS4 method does not address this source of instability explicitly. However, as discussed in Ref. [32], the logarithmic change of variable is generally applicable to any finite element method (see, e.g. [34]); thus, it should be possible to combine the current GLS4 formulation with the log-conformation method to improve the method further.

2. Governing equations

The steady flow of an inertialess incompressible viscoelastic fluid, occupying a spatial domain Ω , with boundary Γ is governed by the momentum and continuity equations:

$$\nabla \cdot \mathbf{T} = \mathbf{0}, \quad \text{on } \Omega, \quad (1)$$

$$\nabla \cdot \mathbf{v} = 0, \quad \text{on } \Omega, \quad (2)$$

where \mathbf{v} is the liquid velocity and \mathbf{T} is the stress tensor, which can be decomposed into a constitutively undetermined isotropic contribution related to incompressibility, and viscous and elastic contributions:

$$\mathbf{T} = -p\mathbf{I} + \boldsymbol{\tau} + \boldsymbol{\sigma}, \quad (3)$$

respectively, where p is the pressure, \mathbf{I} the identity tensor, $\boldsymbol{\tau} = 2\eta_s \mathbf{D}$ the viscous stress (usually due to solvent contribution), η_s the solvent viscosity, and \mathbf{D} is the rate-of-strain tensor, i.e., the symmetric part of the velocity gradient. In order to transform the equations of motion into a set of first-order partial differential equations (necessary for developing a consistent LS formulation for low-order elements), an additional variable \mathbf{L} is introduced to represent the velocity gradient:

$$\mathbf{L} = \nabla \mathbf{v} - \frac{1}{\text{tr} \mathbf{I}} (\nabla \cdot \mathbf{v}) \mathbf{I}, \quad (4)$$

where tr denotes trace.

The last term in Eq. (4) ensures that \mathbf{L} remains traceless even in the finite-precision solution [22]; with this definition, $\mathbf{D} \equiv (\mathbf{L} + \mathbf{L}^T)/2$. In the Oldroyd-B model, the elastic stress is related to the dimensionless conformation tensor \mathbf{M} through a simple linear relationship $\boldsymbol{\sigma} = G(\mathbf{M} - \mathbf{I})$, where $G = \eta_p/\lambda$ is the elastic modulus, η_p the polymer contribution to the viscosity, and λ is the relaxation time. The conformation tensor obeys a hyperbolic evolution equation:

$$\overset{\nabla}{\lambda} \mathbf{M} + (\mathbf{M} - \mathbf{I}) = 0, \quad (5)$$

where $\overset{\nabla}{\mathbf{M}}$ denotes an upper-convected derivative:

$$\overset{\nabla}{\mathbf{M}} = \mathbf{v} \cdot \nabla \mathbf{M} - \mathbf{L}^T \cdot \mathbf{M} - \mathbf{M} \cdot \mathbf{L}. \quad (6)$$

The equations governing the flow can be recast in dimensionless form as:

$$\nabla^* \cdot \mathbf{T}^* = \mathbf{0}, \quad (7)$$

$$\nabla^* \cdot \mathbf{v}^* = 0, \quad (8)$$

$$\mathbf{L}^* - \nabla^* \mathbf{v}^* + \frac{1}{\text{tr} \mathbf{I}} (\nabla^* \cdot \mathbf{v}^*) \mathbf{I} = \mathbf{0}, \quad (9)$$

$$Wi \overset{\nabla}{\mathbf{M}} + (\mathbf{M} - \mathbf{I}) = \mathbf{0}, \quad (10)$$

where $\mathbf{v}^* = \mathbf{v}/v_c$, $p^* = p/(\eta v_c/l_c)$ and $\mathbf{L}^* = \mathbf{L}/(v_c/l_c)$ are dimensionless velocity, pressure and interpolated traceless velocity gradient tensor, respectively. $\nabla^* = \nabla/l_c$ is the dimensionless gradient operator, v_c is a characteristic velocity, and l_c is a characteristic length. The dimensionless Weissenberg number is $Wi = \lambda(v_c/l_c)$. The dimensionless stress tensor \mathbf{T}^* is

$$\mathbf{T}^* = -p^* \mathbf{I} + \beta(\mathbf{L}^* + \mathbf{L}^{*T}) + \frac{1-\beta}{Wi} (\mathbf{M} - \mathbf{I}), \quad (11)$$

where $\beta = \frac{\eta_s}{\eta_s + \eta_p}$ is the viscosity ratio. Hereafter, all variables are dimensionless and the (*) is omitted for clarity.

Boundary conditions on the momentum equation are needed on the entire boundary $\Gamma = \Gamma_g \cup \Gamma_h$. The essential and natural boundary conditions are represented as

$$\mathbf{v} = \mathbf{g} \quad \text{on } \Gamma_g, \quad (12)$$

$$\mathbf{n} \cdot \mathbf{T} = \mathbf{h} \quad \text{on } \Gamma_h, \quad (13)$$

where \mathbf{g} and \mathbf{h} are given functions, and \mathbf{n} is the outward unit vector normal to the boundary. Because the equation of transport of conformation is hyperbolic, boundary conditions on the conformation tensor, represented by the tensor \mathbf{G} , are imposed at inflow boundaries Γ_G where $\mathbf{v} \cdot \mathbf{n} < 0$,

$$\mathbf{M} = \mathbf{G} \quad \text{on } \Gamma_G. \quad (14)$$

3. Four-field Galerkin/least-squares formulation (GLS4)

In this section, the GLS formulation of the governing equations (7)–(10) is presented. The method is termed GLS4 because the equation set has four basic unknown fields— \mathbf{v} , p , \mathbf{L} and \mathbf{M} . The basis (interpolation) and weighting function spaces are:

$$\mathcal{S}_v^h = \{\mathbf{v}^h | \mathbf{v}^h \in [H^{1h}(\Omega)]^{n_{sd}}, \quad \mathbf{v}^h \equiv \mathbf{g}^h \text{ on } \Gamma_g\}, \quad (15)$$

$$\mathcal{V}_v^h = \{\mathbf{v}^h | \mathbf{v}^h \in [H^{1h}(\Omega)]^{n_{sd}}, \quad \mathbf{v}^h \equiv \mathbf{0} \text{ on } \Gamma_g\}, \quad (16)$$

$$\mathcal{S}_p^h = \mathcal{V}_p^h = \{p^h | p^h \in H^{1h}(\Omega)\}, \quad (17)$$

$$\mathcal{S}_L^h = \mathcal{V}_L^h = \{\mathbf{L}^h | \mathbf{L}^h \in [H^{1h}(\Omega)]^{n_{sd}^2}\}, \quad (18)$$

$$\mathcal{S}_M^h = \{\mathbf{M}^h | \mathbf{M}^h \in [H^{1h}(\Omega)]^{n_{tc}}, \quad \mathbf{M}^h \equiv \mathbf{G} \text{ on } \Gamma_G\}, \quad (19)$$

$$\mathcal{V}_M^h = \{\mathbf{M}^h | \mathbf{M}^h \in [H^{1h}(\Omega)]^{n_{tc}}, \quad \mathbf{M}^h \equiv \mathbf{0} \text{ on } \Gamma_G\}, \quad (20)$$

where H^{1h} represents functions with square integrable first-order derivatives, n_{sd} the number of spatial dimensions and $n_{tc} = n_{sd}(n_{sd} + 1)/2$ is the number of independent conformation tensor components. Bilinear piecewise continuous functions are used hereafter. The GLS4 formulation is: Find $\mathbf{v}^h \in \mathcal{S}_v^h$, $p^h \in \mathcal{S}_p^h$, $\mathbf{L}^h \in \mathcal{S}_L^h$ and $\mathbf{M}^h \in \mathcal{S}_M^h$ such that:

$$\begin{aligned} & \int_{\Omega} \nabla \mathbf{w}^h : \mathbf{T}^h \, d\Omega + \int_{\Gamma_h} \mathbf{w}^h \cdot \mathbf{h}^h \, d\Gamma \\ & + \int_{\Omega} \tau_{\text{mom}} \left[\nabla q^h - \beta \nabla \cdot (\mathbf{E}^h + (\mathbf{E}^h)^T) - \underbrace{\frac{1-\beta}{Wi} \nabla \cdot \mathbf{S}^h}_A \right] \\ & \quad [-\nabla \cdot \mathbf{T}^h] \, d\Omega + \int_{\Omega} q^h (\nabla \cdot \mathbf{v}^h) \, d\Omega \\ & + \int_{\Omega} \tau_{\text{cont}} (\nabla \cdot \mathbf{w}^h) (\nabla \cdot \mathbf{v}^h) \, d\Omega \\ & + \int_{\Omega} \mathbf{E}^h : \left[\mathbf{L}^h - \nabla \mathbf{v}^h + \frac{1}{\text{tr} \mathbf{I}} (\nabla \cdot \mathbf{v}^h) \mathbf{I} \right] \, d\Omega \\ & + \int_{\Omega} \tau_{\text{gradv}} \left[\mathbf{E}^h - \nabla \mathbf{w}^h + \frac{1}{\text{tr} \mathbf{I}} (\nabla \cdot \mathbf{w}^h) \mathbf{I} \right] : \left[\mathbf{L}^h - \nabla \mathbf{v}^h \right. \\ & \quad \left. + \frac{1}{\text{tr} \mathbf{I}} (\nabla \cdot \mathbf{v}^h) \mathbf{I} \right] \, d\Omega + \int_{\Omega} \mathbf{S}^h : \left[Wi (\mathbf{v}^h \cdot \nabla \mathbf{M}^h - (\mathbf{L}^h)^T \cdot \mathbf{M}^h \right. \\ & \quad \left. - \mathbf{M}^h \cdot \mathbf{L}^h) + (\mathbf{M}^h - \mathbf{I}) \right] \, d\Omega + \int_{\Omega} \tau_{\text{cons}} \left[Wi (\mathbf{v}^h \cdot \nabla \mathbf{S}^h \right. \end{aligned}$$

$$\begin{aligned}
& -(\mathbf{L}^h)^T \cdot \mathbf{S}^h - \mathbf{S}^h \cdot \mathbf{L}^h + \mathbf{S}^h \Big] : \left[Wi(\mathbf{v}^h \cdot \nabla \mathbf{M}^h - (\mathbf{L}^h)^T \cdot \mathbf{M}^h \right. \\
& \left. - \mathbf{M}^h \cdot \mathbf{L}^h) + (\mathbf{M}^h - \mathbf{I}) \right] d\Omega = 0, \\
& \nabla q^h \in \mathcal{V}_p^h, \nabla \mathbf{w}^h \in \mathcal{V}_v^h, \nabla \mathbf{E}^h \in \mathcal{V}_L^h, \nabla \mathbf{S}^h \in \mathcal{V}_M^h,
\end{aligned} \quad (21)$$

where τ_{mom} , τ_{cont} , τ_{gradv} and τ_{cons} are the LS stabilization parameters for the momentum, continuity, interpolated traceless velocity gradient and constitutive equations, respectively. The underbraced term A is neglected at low Wi because the $(1/Wi)$ term grows large as $Wi \rightarrow 0$, causing numerical problems.

3.1. Design of the stabilization coefficients

The appropriate design of the four stabilization parameters — τ_{mom} , τ_{cont} , τ_{gradv} and τ_{cons} — in Eq. (21) plays a crucial role in the performance of the method.

The τ_{mom} -term stabilizes the Galerkin form in advection-dominated flows, and also removes the compatibility condition between velocity and pressure spaces. The parameter designed specifically for use with bilinear interpolations [31] is adapted here for the dimensionless system:

$$\tau_{\text{mom}} = \frac{h^2}{4}. \quad (22)$$

where h is the dimensionless element length.

The τ_{cont} -term improves the convergence of non-linear solvers in advection-dominated problems. Hereafter, $\tau_{\text{cont}} = 0$ because inertia is neglected.

The τ_{gradv} -term stabilizes Eq. (4); although the associated stabilization term is not strictly necessary, τ_{gradv} is taken here as $\tau_{\text{gradv}} = 1$.

The τ_{cons} -term is introduced to stabilize the Galerkin form at high Wi , and to bypass the compatibility conditions between velocity and conformation spaces. No systematic derivation for τ_{cons} is available in the literature. However, the transport equation of conformation can be viewed as an advection-generation equation, and considerable research has been done on stabilization parameters for a simple advection-diffusion-generation equation [35–39]. Applying the definition proposed by Franca et al. [38], based on the convergence and stability analysis of advection-diffusion-generation equation, and extended by Hauke [39], yields

$$\tau_{\text{cons1}} = 1, \quad (23)$$

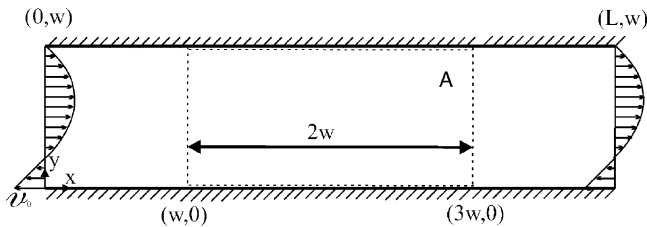


Fig. 1. Schematic of a flow in a planar channel with $w/L = 1/4$. The top wall is kept fixed, the bottom wall is moving from right to left at v_0 and a differential pressure is applied between the left and right walls.

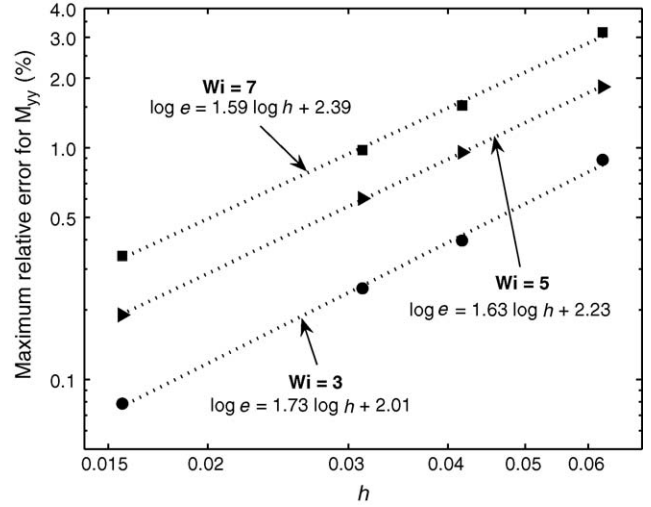


Fig. 2. Mesh-convergence rate for a planar channel flow at different Wi . The slope of the curves gives the rate of convergence with mesh refinement.

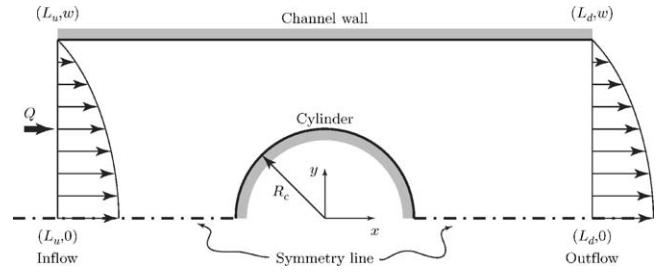


Fig. 3. Geometry of a flow past a cylinder in a half channel.

$$\tau_{\text{cons2}} = \frac{1}{Wi \|\mathbf{L}^h\|}, \quad (24)$$

$$\tau_{\text{cons3}} = \frac{h}{2Wi \|\mathbf{v}^h\|}. \quad (25)$$

τ_{cons1} and τ_{cons2} are important in regions of the flow where generation is dominant, whereas τ_{cons3} is important in advection-dominated regions. These three contributions can be combined

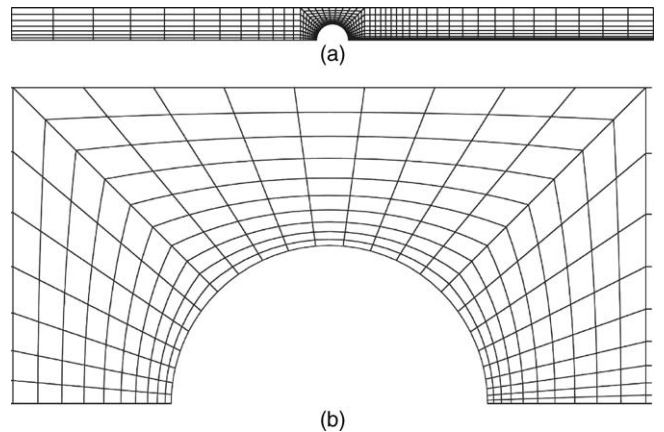


Fig. 4. Flow past a cylinder in a channel, $w/R_c = 2$: Finite element mesh M0 (a) complete domain (b) detail of the mesh from $x = -2$ to $x = 2$.

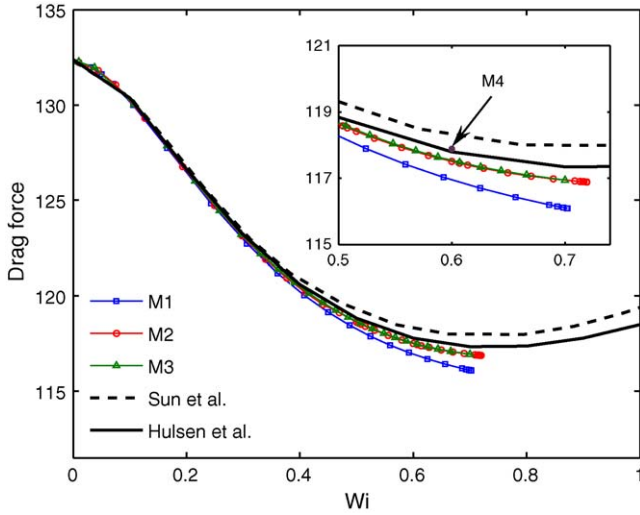


Fig. 5. (Color online) Flow past a cylinder in a channel, $w/R_c = 2$: drag force on the cylinder versus Wi . The GLS4 results for the four meshes (M1, M2, M3 and M4) are compared with the results presented by Sun et al. [21] and Hulsén et al. [34]. Inset: detail of the drag force at high Wi . ● represents the drag force on M4 at $Wi = 0.6$. At $Wi = 0.6$, the extrapolated value of the drag force is 117.979, which is within 0.2% of the values reported in Refs. [30,34,40].

as:

$$\tau_{\text{cons}} = \left(\frac{1}{\tau_{\text{cons}1}^r} + \frac{1}{\tau_{\text{cons}2}^r} + \frac{1}{\tau_{\text{cons}3}^r} \right)^{-1/r}, \quad (26)$$

Hereafter, the switching parameter is set to $r = 2$ (see also Ref. [29]):

$$\tau_{\text{cons}} = \left[1 + (Wi \|\mathbf{L}^h\|)^2 + \left(\frac{2Wi \|\mathbf{v}^h\|}{h} \right)^2 \right]^{-1/2}. \quad (27)$$

4. Numerical results

The proposed GLS4 formulation is tested in flow in a planar channel and flow past a cylinder in a channel. An analytical solution can be obtained in the former case; in the latter, the

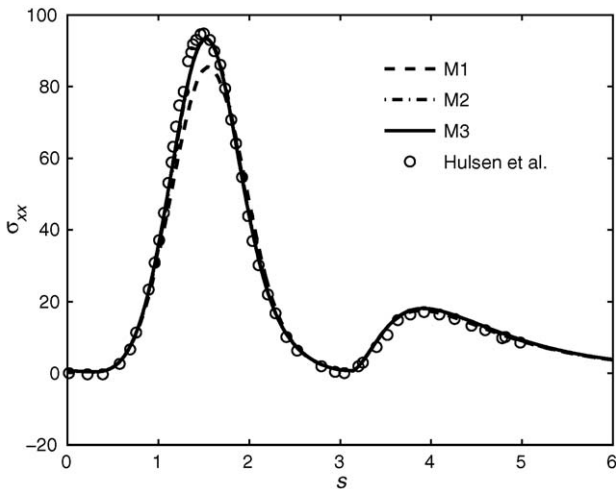


Fig. 6. Flow past a cylinder in a channel, $w/R_c = 2$: σ_{xx} on the cylinder and on the symmetry line in the wake at $Wi = 0.6$. ○ from Hulsén et al. [34].

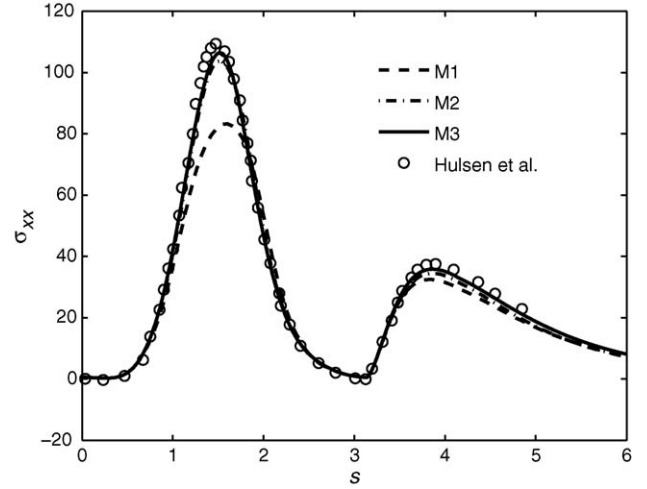


Fig. 7. Flow past a cylinder in a channel, $w/R_c = 2$: σ_{xx} on the cylinder and on the symmetry line in the wake at $Wi = 0.7$. ○ from Hulsén et al. [34].

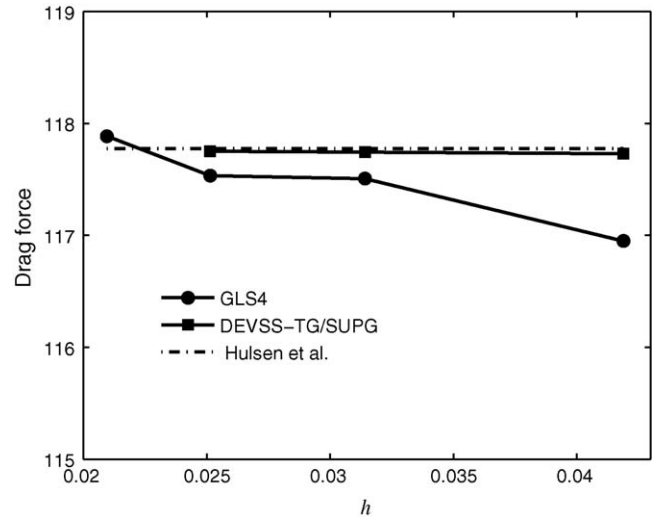


Fig. 8. Flow past a cylinder in a channel, $w/R_c = 2$: Drag force at $Wi = 0.6$ for GLS4 and DEVSS-TG/SUPG for all meshes; dashed line represents the drag force reported by Hulsén et al. [34] on their finest mesh.

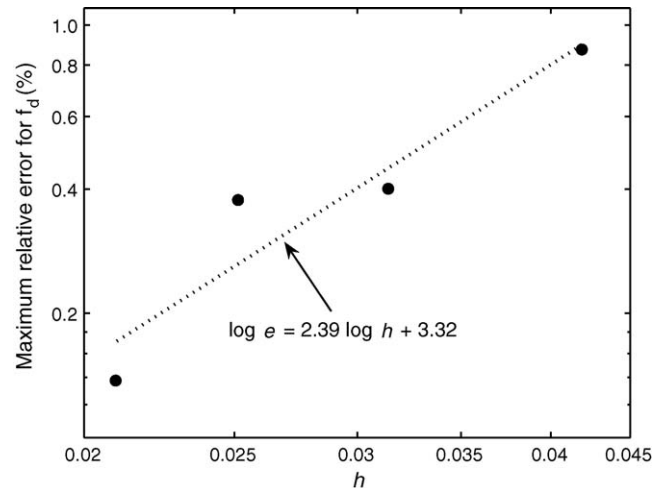


Fig. 9. Flow past a cylinder in a channel, $w/R_c = 2$: Mesh-convergence rate of the drag force at $Wi = 0.6$.

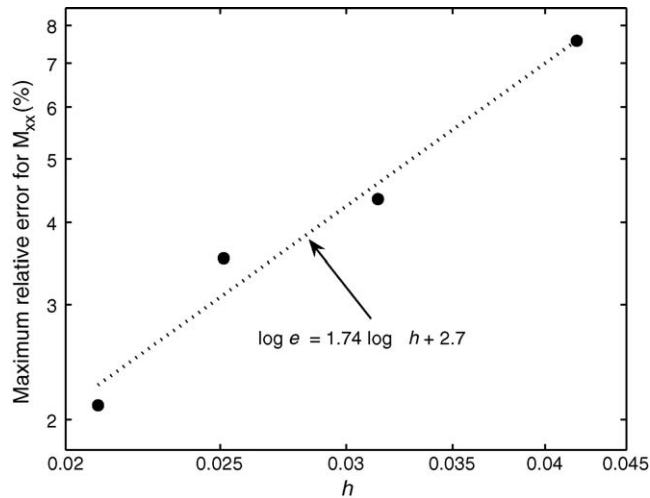


Fig. 10. Flow past a cylinder in a channel, $w/R_c = 2$: Mesh-convergence rate of M_{xx} at a point in the wake flow ($x = 2$; $y = 0$) at $Wi = 0.6$.

numerical results from other state-of-the-art methods are used for validation [20–22,29,34,40]. The flow past a cylinder in a channel is a standard benchmark problem with desirable characteristics of smooth boundaries, and poses several numerical challenges at high Wi due to the formation of sharp boundary layers on the cylinder and in the wake.

4.1. Flow in a planar channel

Fig. 1 shows a combination of Poiseuille flow (pushing liquid from left to right) and Couette flow (induced by the bottom wall dragging liquid from right to left with velocity v_0) in a planar channel of width $w = 1$ and length $L = 4w$. The flow of an Oldroyd-B fluid ($\beta = 0.59$) is simulated, and the results are compared with the known analytical solution. The figure also shows velocity profiles at the two open flow boundaries; both right and left ends of the channel have respective inflow and outflow sections. A region ‘A’ (dotted area in Fig. 1), which is $2w$ in length and centrally placed in the channel, is monitored for comparing numerical results with analytical solution; this sufficiently eliminates the influences due to the boundary conditions. The problem setup closely follows the numerical example employed by Xie and Pasquali [41]; the analytical solution for velocity and conformation fields are

$$v_x = \left[-\frac{\Delta p}{2} \frac{w}{L} \left[\left(\frac{y}{w} \right)^2 - \frac{y}{w} \right] + \frac{y}{w} - 1 \right] v_0, \quad v_y = 0, \quad (28)$$

$$M_{xx} = 1 + 2 \left(\lambda \frac{dv_x}{dy} \right)^2, \quad M_{xy} = \lambda \frac{dv_x}{dy}, \quad M_{yy} = 1, \quad (29)$$

where $\Delta p = 50$ is the differential pressure between the left and right boundaries. Consequently, $Wi = \lambda[\Delta p w/(2L) + 1](v_0/w)$. The Dirichlet conditions are imposed for velocity components on all boundaries, and the conformation tensor components are only specified at the corresponding inflows. The numerical results are obtained on four different uniform meshes — 16×16 , 24×24 , 32×32 and 64×64 — followed by a node-by-node

computation of the relative errors $e = |(\text{numerical value} - \text{analytical value})/(\text{analytical value})| \times 100\%$ in region A. Fig. 2 shows the maximum e in M_{yy} (which has the highest e among all unknown fields) versus the element size for $Wi = 3, 5$ and 7 . From the three curves the rate of mesh convergence is estimated to be 1.73, 1.63 and 1.59, respectively. Because increase in Wi results in increased generation, subsequently forming steeper boundary layer close to the channel walls, the rate of convergence is found to decrease. At $Wi = 3$, Xie and Pasquali [41] reported a rate of convergence of 1.89 using DEVSS-TG/SUPG method with bi-quadratic interpolation for velocity.

4.2. Flow past a cylinder in a channel

The flow of an Oldroyd-B fluid past a cylinder in a rectangular channel has been used as a standard benchmark problem to test several computational methods [20–22,29,34,40]. For computational ease, the symmetry of the problem is used and only half of the channel is simulated. Fig. 3 shows the schematic of the problem, where L_u , L_d , R_c and w represent the upstream length, the downstream length, the cylinder radius, and the half channel width, respectively.

A no-slip boundary condition is imposed on the cylinder surface and channel walls, and fully developed flow conditions are assumed at the inflow and outflow boundaries. Consequently:

$$v_x = 1.5 \frac{Q}{w} \left(1 - \frac{y^2}{w^2} \right), \quad v_y = 0, \quad (30)$$

$$M_{xx} = -3 \frac{Q}{w} \lambda \frac{y}{w^2}, \quad M_{xy} = M_{yx} = 1 - 2 \left(-\frac{3Q\lambda y}{w^3} \right)^2, \\ M_{yy} = 1, \quad (31)$$

where Q is the flow rate. Whereas the velocity is imposed at both inflow and outflow, the conformation tensor components are specified at the inflow only. At the symmetry line, $\mathbf{n} \cdot \mathbf{T} = \mathbf{0}$ and $v_y = 0$, where \mathbf{n} is the unit vector normal to the symmetry line. The computed drag on the cylinder f_d has been traditionally used to compare numerical methods:

$$f_d = -2 \int_S \mathbf{e}_1 \mathbf{n} : \mathbf{T} dS, \quad (32)$$

where S represents the surface of the cylinder, \mathbf{n} the unit normal vector, and \mathbf{e}_1 is the unit vector in the x -direction.

4.2.1. Flow past a cylinder in a channel: $w/R_c = 2$

In this case, $w = 2$, $R_c = 1$, $L_u = -20$, $L_d = 20$, $Q = 2$ and $\beta = 0.59$. Fig. 4 shows the mesh M0 from which four systematically refined meshes are obtained; in these meshes, the elements are concentrated on the cylinder surface and in the wake along the symmetry line. The M1, M2, M3 and M4 meshes are obtained by dividing every element side of M0 by 3, 4, 5 and 6, respectively. The number of elements and corresponding number of unknowns are listed in Table 1. This flow problem poses numerical challenges at high Wi ; therefore, the maximum Wi up to which the numerical schemes converge has been employed as a measure of robustness (but not necessarily accuracy). For

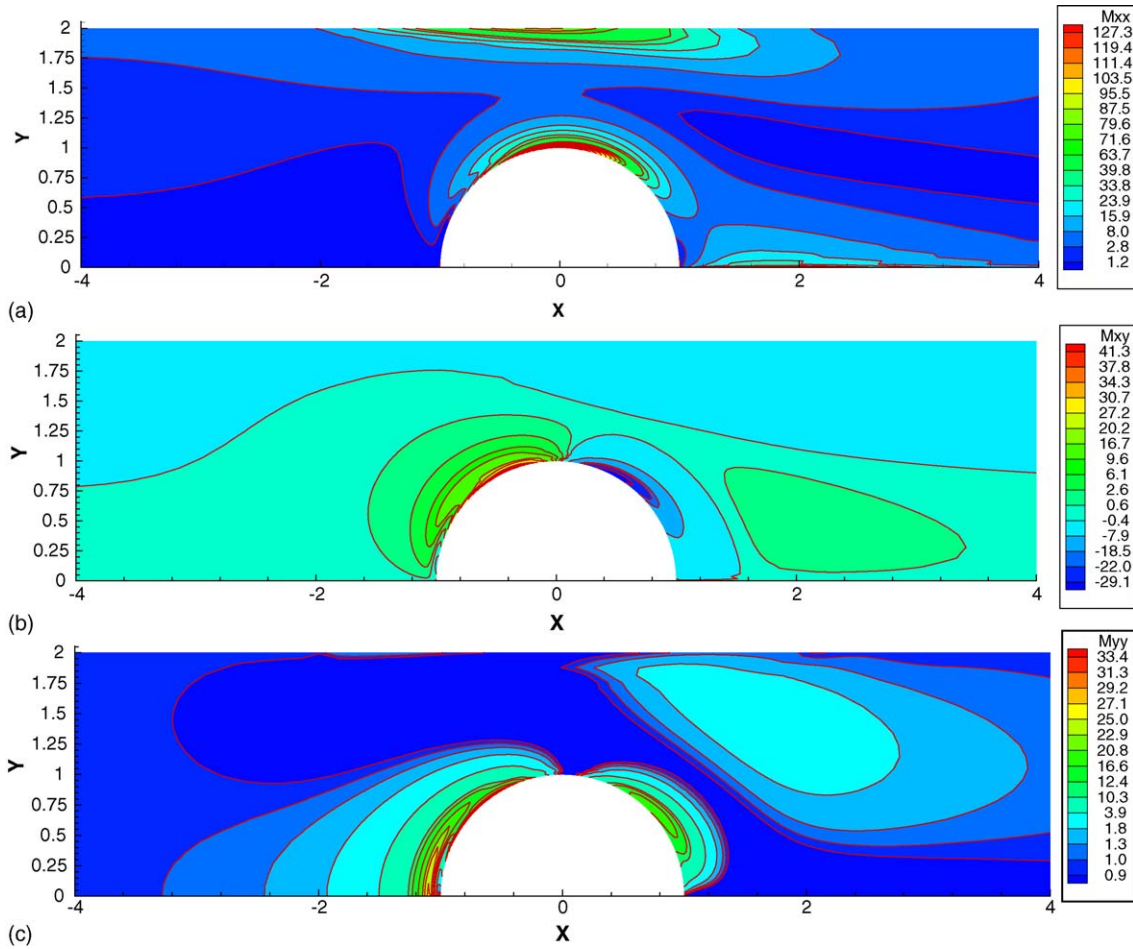


Fig. 11. (Color online) Flow past a cylinder in a channel, $w/R_c = 2$: (a) M_{xx} , (b) M_{xy} and (c) M_{yy} contours at $Wi = 0.7$ on mesh M2.

example, using DEVSS-G/SUPG, Sun et al. [21] reported solutions up to $Wi = 1.85$, Fan et al. [30] using an incomplete GLS up to $Wi = 1.05$ and Hulsén et al. [34] using the log conformation up to $Wi = 2.0$; however, the accuracy of the solutions at $Wi > 0.6$ was not confirmed in these works.

Here, a sequence of flow states is computed by first-order arc-length continuation on Wi with automatic step control; the continuation terminates when the conformation tensor loses its positive-definiteness, which occurs at $Wi \sim 0.7$. The positive-definiteness of \mathbf{M} was not usually considered in past stud-

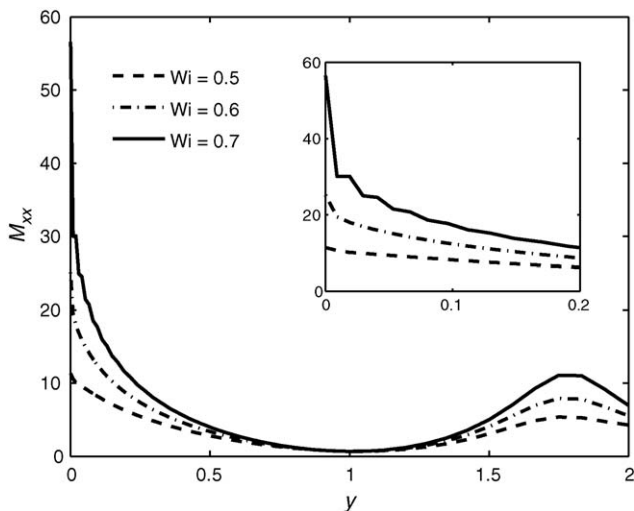


Fig. 12. Flow past a cylinder in a channel, $w/R_c = 2$: M_{xx} along line $x = 2$ on mesh M3. Inset: detail of M_{xx} near the centerline ($y = 0$).

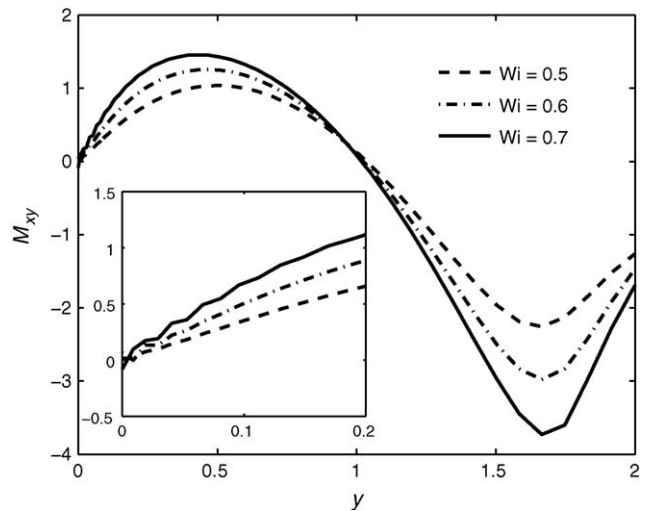


Fig. 13. Flow past a cylinder in a channel, $w/R_c = 2$: M_{xy} along line $x = 2$ on mesh M3. Inset: detail of M_{xy} near the centerline ($y = 0$).

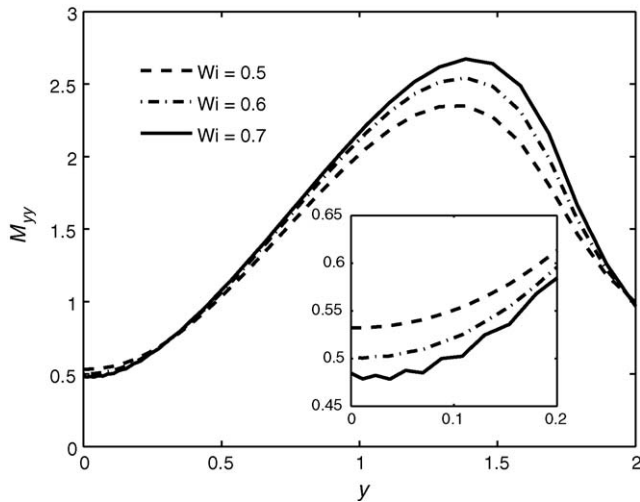


Fig. 14. Flow past a cylinder in a channel, $w/R_c = 2$: M_{yy} along line $x = 2$ for M3. Inset: detail of M_{yy} near the centerline ($y = 0$).

ies, with exception of the recent work of Hulsen et al. [34]. Fig. 5 shows the drag forces on the meshes M1, M2 and M3; a good agreement is found up to $Wi = 0.4$ with the results reported by Hulsen et al. [34] and Sun et al. [21]. Beyond that, the three methods show slight differences in the drag predictions, while following the same trend. Figs. 6 and 7 show σ_{xx} versus s at $Wi = 0.6$ and 0.7 , respectively, where $\sigma_{xx} = (\eta_p/\lambda)M_{xx}$ and s is defined as: $0 < s < \pi R_c$ on the cylinder and $\pi R_c < s < \pi R_c + L_d - R_c$ in the wake along the symmetry line. At $Wi < 0.6$, a complete overlap is observed among the results on the meshes M1, M2 and M3. In Fig. 6, σ_{xx} profiles computed with M1, M2 and M3 are overlapping in the wake; however, the result from M1 shows underprediction on the cylinder, implying that refinement of M1 is not sufficient to capture the steep boundary layer on the cylinder. On the other hand, in Fig. 7, differences are observed not only on the cylinder but also in the wake flow. The figures also show the results reported by Hulsen et al. [34] at the corresponding Wi ,

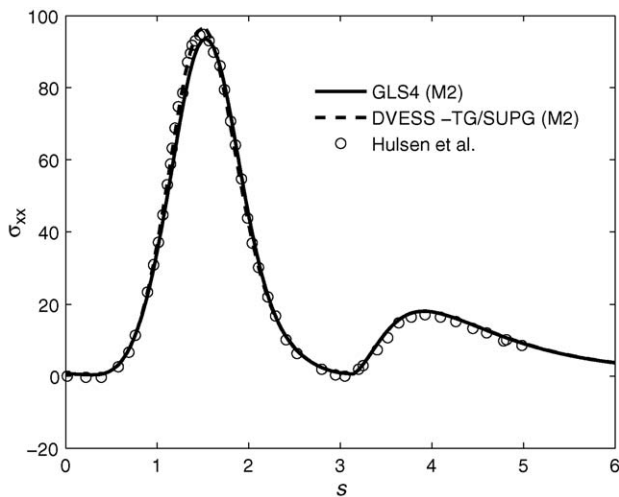


Fig. 15. Flow past a cylinder in a channel, $w/R_c = 2$: σ_{xx} on the cylinder and on the symmetry line at $Wi = 0.6$. The GLS4 and DEVSS-TG/SUPG results are obtained for M2. \circ from Hulsen et al. [34].

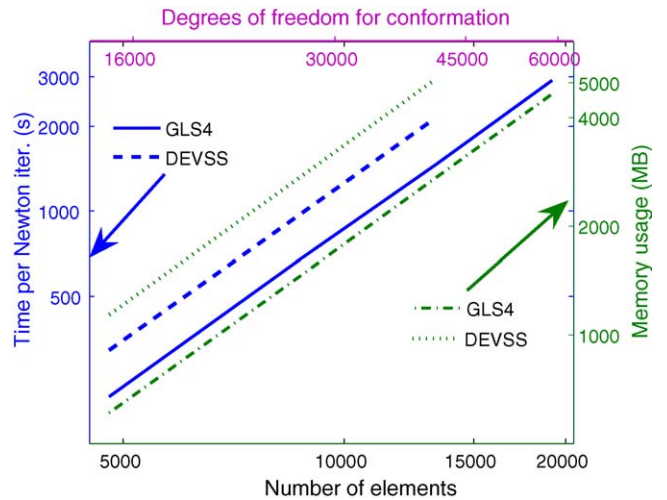


Fig. 16. (Color online) Direct comparison of GLS4 and DEVSS-TG/SUPG with respect to the number of elements (bottom axis) and to the number of degrees of freedom for conformation (top axis). The left and right axes represent the time per Newton iteration (s) and memory usage (MB), respectively. A frontal solver is used in both simulations.

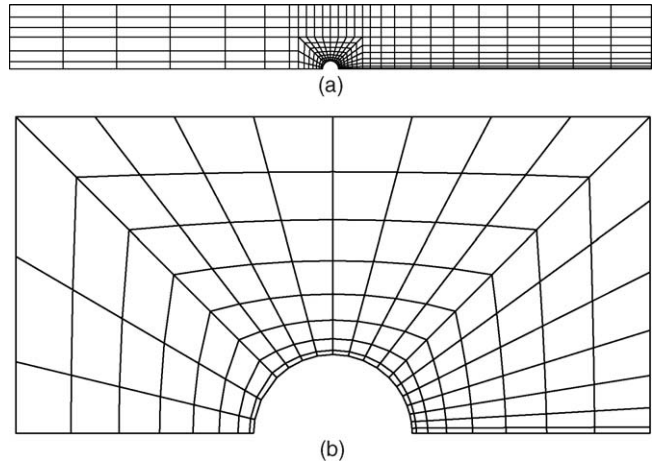


Fig. 17. Flow past a cylinder in a channel, $w/R_c = 8$: Finite element mesh M0 (a) complete domain (b) detail of the mesh from $x = -4$ to $x = 4$.

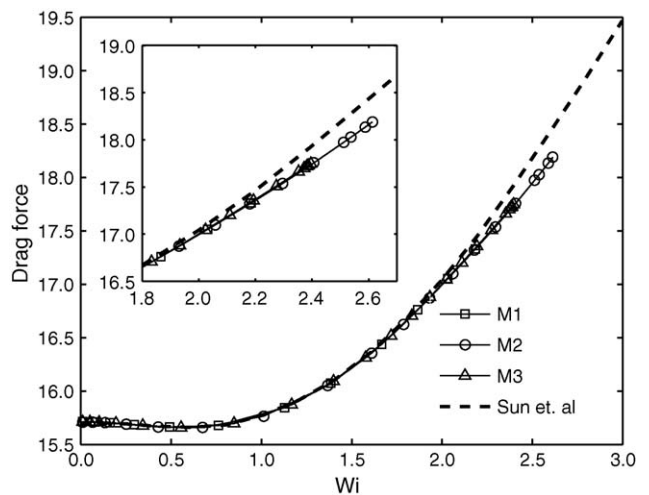


Fig. 18. Flow past a cylinder in a channel, $w/R_c = 8$: Drag force on the three meshes. The dotted curve is obtained from Sun et al. [21]. Inset: detail of the drag force at high Wi .

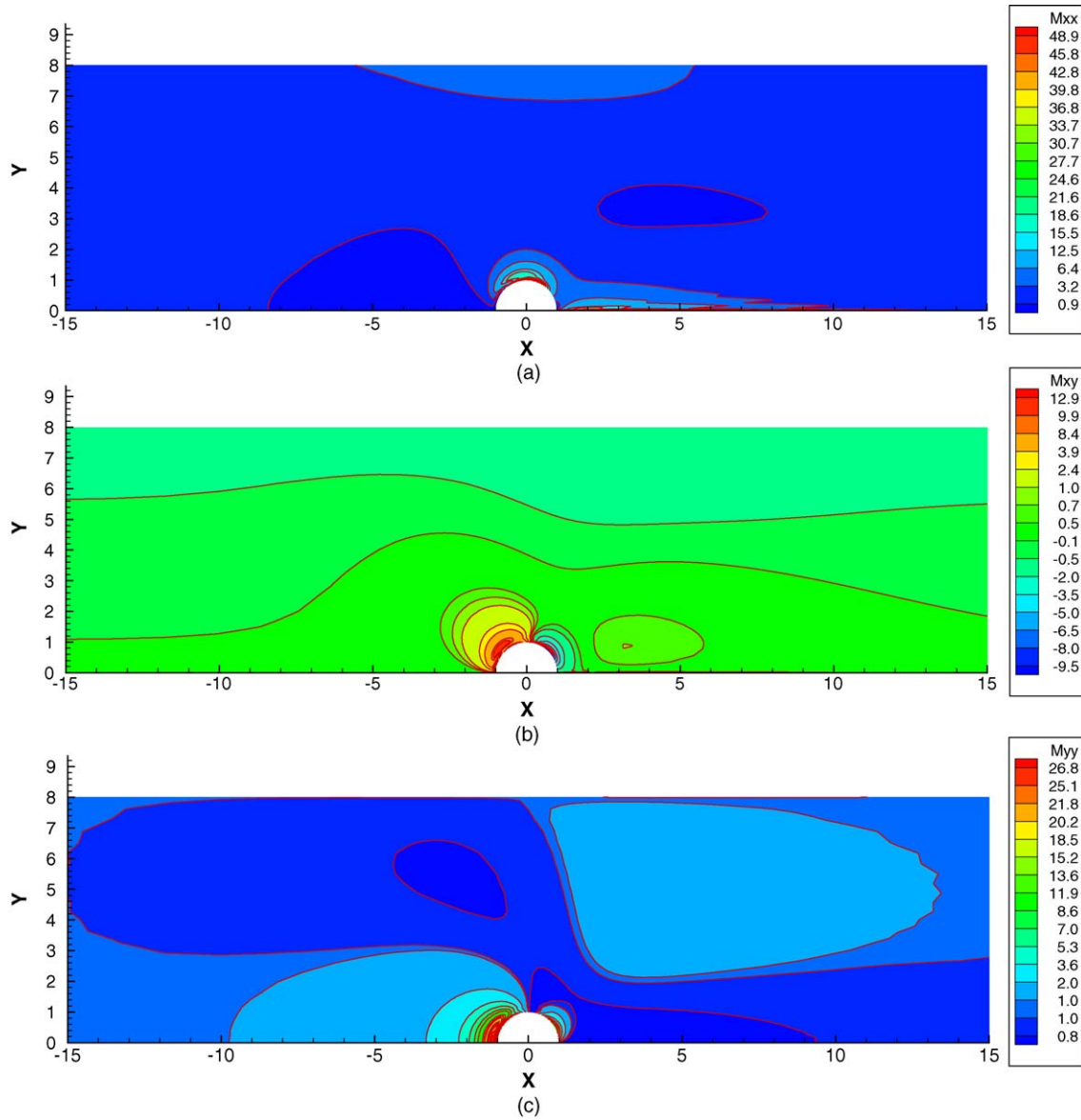


Fig. 19. (Color online) Flow past a cylinder in a channel, $w/R_c = 8$: (a) M_{xx} , (b) M_{xy} and (c) M_{yy} contours at $Wi = 2.0$ on mesh M2.

Table 1
Flow past a cylinder in a channel, $w/R_c = 2$: Characteristics of the finite element meshes

Mesh	Elements	Unknowns		Time per Newton iteration (s)			Memory usage (MB)		
		GLS4	DEVSS	GLS4	DEVSS	ϵ_d	GLS4	DEVSS	ϵ_d
M0	532	–	–	–	–	–	–	–	–
M1	4788	49960	79102	220	322	31.7	608	1140	46.7
M2	8512	87890	139514	648	934	30.6	1410	2647	46.7
M3	13300	136460	216950	1460	2144	31.9	2720	5122	46.9
M4	19152	195670	311410	2914	–	–	4650	–	–

ϵ_d is the % relative difference in the respective values from DEVSS and GLS4.

Table 2
Flow past a cylinder in a channel, $w/R_c = 8$: Characteristics of the finite element meshes

Mesh	Elements	Unknowns	Time per Newton iteration (s)	Memory usage (MB)
M0	250	–	–	–
M1	4000	41690	198	396
M2	6250	64610	440	863
M3	12250	125450	1505	1859

and good agreement is found with results on M3. In previous works, the convergence of the stresses has been shown by comparing stress profiles obtained on systematically refined meshes using p- and h-refinement [30,34]. While overlap of the results demonstrates qualitatively mesh convergence, here, accuracy is measured more precisely by Richardson extrapolation:

$$f_d(h) = f_d(0) + \alpha h^n, \quad (33)$$

where $f_d(0)$ is the drag for an infinitely refined mesh, n the rate of mesh convergence and α is a constant. $f_d(0)$ is used to compute the relative errors $e = |(f_d(h) - f_d(0))/f_d(0)| \times 100\%$ in $f_d(h)$. Fig. 8 shows f_d predictions from GLS4 and DEVSS-TG/SUPG along with the results presented by Hulsen et al. [34] at $Wi = 0.6$. The extrapolated values of f_d for an infinitely refined mesh are 117.979 and 117.778 for GLS4 and DEVSS-TG/SUPG, respectively. Thus, the GLS4 extrapolated results are within 0.2% of the values computed by high resolution finite volume ($f_d = 117.79$ [40]), by pressure-stabilized finite elements ($f_d = 117.78$ [30]), by DEVSS-DG-Log conformation finite elements ($f_d = 117.77$ [34]), and by DEVSS-TG/SUPG calculations. Fig. 9 shows e versus h , and a mesh convergence rate of 2.39 is observed.

Similarly, Richardson extrapolation analysis is also performed for M_{xx} at a point in the wake flow ($x = 2; y = 0$). The extrapolated value of M_{xx} is 26.05 and the rate of mesh convergence is 1.74. Fig. 10 shows e versus h for M_{xx} . In all cases, results on M4 are also employed to obtain the extrapolated values. Fig. 11 shows the conformation contours at $Wi = 0.7$, in which, the formation of sharp boundary layers on the cylinder and along the symmetry line in the wake flow are observed. These boundary layers are difficult to resolve numerically, and the onset of oscillations in the conformation fields is observed as the boundary layers grow at high Wi . The influence of the sharp boundary layer at high Wi is shown in Figs. 12–14, which plot \mathbf{M} components along line $x = 2$. At $Wi = 0.5$ and 0.6 a smooth profile for the \mathbf{M} components is observed, whereas at $Wi = 0.7$ oscillations appear towards the symmetry line ($y \rightarrow 0$). The maximum Wi attained in these simulations is slightly above 0.7; beyond this, \mathbf{M} loses its positive-definiteness.

A direct comparison of computational cost between GLS4 and DEVSS-TG/SUPG is performed, while keeping the same number of degrees of freedom for conformation; the latter employs biquadratic interpolation functions for velocity, whereas bilinear for pressure, velocity gradient and conformation. The results at $Wi = 0.6$ on M2 are obtained from both methods and comparable accuracy is observed. Fig. 15 shows σ_{xx} versus s along with the results of Hulsen et al. [34]. The GLS4 and DEVSS-TG/SUPG characteristics (number of unknowns, time per Newton iteration and memory usage) are listed in Table 1.

Fig. 16 shows a direct comparison of GLS4 and DEVSS-TG/SUPG with respect to the number of degrees of freedom for conformation, and it can be observed that GLS4 is $\sim 30\%$ computationally faster and uses only 45% of the memory compared to DEVSS-TG/SUPG (for the same number of degrees of freedom for conformation).

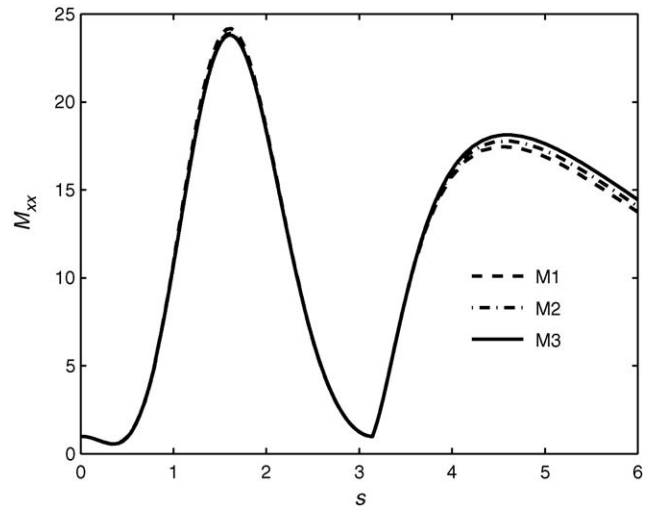


Fig. 20. Flow past a cylinder in a channel, $w/R_c = 8$: M_{xx} on the cylinder and along the symmetry line in the wake at $Wi = 1.5$.

4.2.2. Flow past a cylinder in a channel: $w/R_c = 8$

In this case, $w = 8$, $R_c = 1$, $L_u = -40$, $L_d = 40$, $Q = 8$ and $\beta = 0.59$. Following the same procedure as in the previous case, the M1, M2 and M3 meshes are obtained by dividing every element side of the mesh M0 by 4, 5 and 7, respectively. Fig. 17 shows the mesh M0, and details of the subsequent meshes are listed in Table 2. The drag on the cylinder from the three meshes are compared with the results reported by Sun et al. [21] in Fig. 18. For this case, a complete overlap of drag predictions from the three meshes is observed, and a good agreement with results of Sun et al. [21] is found up to $Wi = 2.0$. Moreover, the maximum Wi achieved in this simulation is ~ 2.7 . In Fig. 19, the contour plots for the \mathbf{M} components are shown at $Wi = 2.0$. Figs. 20 and 21 show M_{xx} versus s (defined in Section 4.2.1) at $Wi = 1.5$ and 2.0 , respectively. At $Wi = 2.0$, the streamwise normal conformation component M_{xx} has not yet converged in

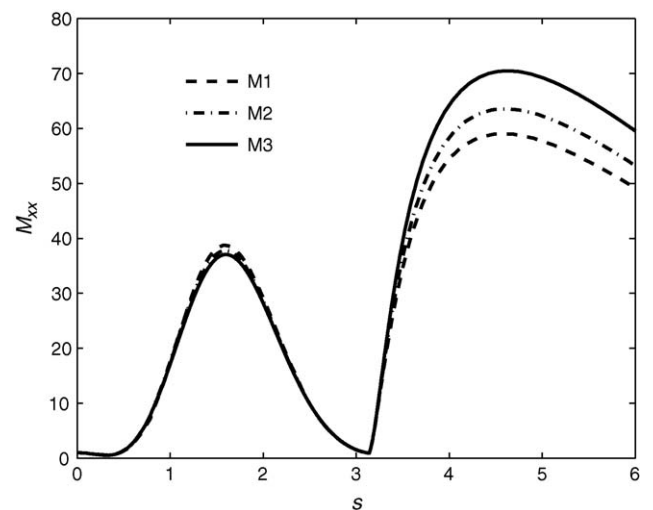


Fig. 21. Flow past a cylinder in a channel, $w/R_c = 8$: M_{xx} on the cylinder and along the symmetry line in the wake at $Wi = 2.0$.

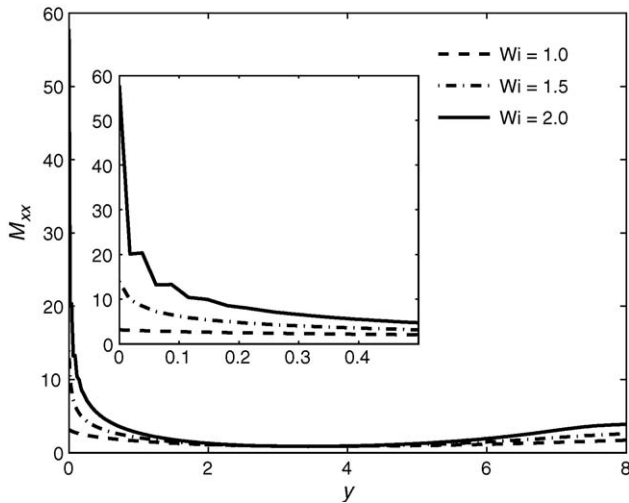


Fig. 22. Flow past a cylinder in a channel, $w/R_c = 8$: M_{xx} along line $x = 4$ on mesh M3.

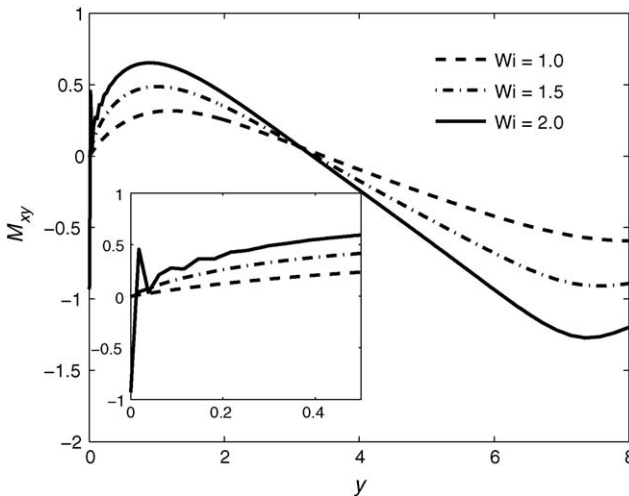


Fig. 23. Flow past a cylinder in a channel, $w/R_c = 8$: M_{xy} along line $x = 4$ on mesh M3.

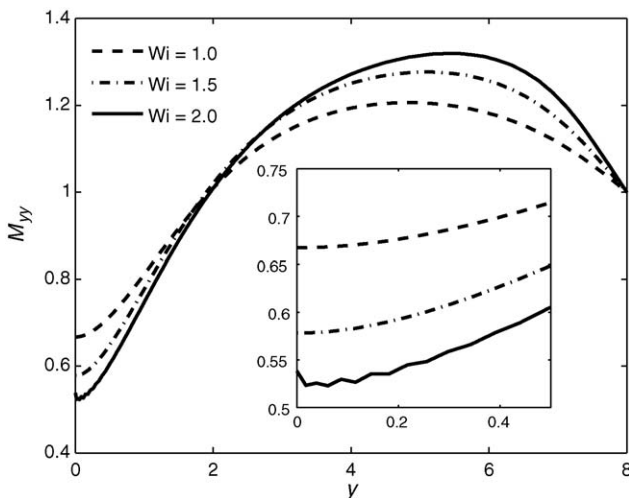


Fig. 24. Flow past a cylinder in a channel, $w/R_c = 8$: M_{yy} along line $x = 4$ on mesh M3.

the wake. Figs. 22–24 show the \mathbf{M} components along the line $x = 4$ at $Wi = 1.0, 1.5$ and 2.0 , respectively. It can be seen that significant oscillations appear towards the symmetry line ($y \rightarrow 0$) at $Wi = 2.0$.

5. Conclusions

A complete four-field Galerkin/Least-Squares (GLS4) formulation to simulate the flow of viscoelastic fluids is presented. The method successfully circumvents the compatibility conditions associated with the multiple discrete unknown fields, thereby allowing equal-order polynomial interpolations for all variables.

The formulation is presented for the equations governing the inertialess flow of an Oldroyd-B ($\beta = 0.59$) fluid. The constitutive equation is written in terms of the conformation tensor, and can be easily extended to other constitutive models (e.g., Giesekus, FENE-P, FENE-CR, etc.). The set of governing equations—conservation of mass, momentum and the constitutive equation—are reduced to first-order by employing an interpolated traceless velocity gradient. The equations are solved in a coupled way by using Newton’s method with analytical Jacobian and a direct solver; the positive-definiteness of the conformation tensor is checked in all simulations. The method is evaluated for obtaining mesh-converged solutions in two benchmark problems.

The flow in a planar channel is computed on four meshes of increasing resolution. The results are compared with the known analytical solution, and it is observed that the GLS4 method is able to preserve the positive-definiteness of \mathbf{M} at high Wi . The mesh-convergence rate is also computed and found to be comparable to the state-of-the-art methods such as DEVSS.

The flow past a cylinder in a channel is computed on systematically refined meshes. Two different ratios of channel width to cylinder radius are used—2:1 and 8:1. In both cases, at moderate Wi , the drag on the cylinder matches well with the state-of-the-art methods, and at high Wi , the results follow the same trends. It is well known that in these problems, sharp boundary layers of \mathbf{M} are formed on the cylinder and along the symmetry line in the wake, therefore mesh convergence for all components of \mathbf{M} is analyzed. The onset of the oscillations in the computed values of conformation are observed at high Wi ; this may be due to the non-optimal definition of the stabilization parameters, or to the failure of the low order basis functions to capture exponentially growing stress (conformation) profiles along streamlines in zones of strong flow (see, e.g., Refs. [33,34]). On single processor machines, GLS4 proves about 30% faster and 50% cheaper (memory-wise) than DEVSS while providing results of comparable accuracy. However, GLS4 is expected to scale better on distributed memory clusters because of nodal accounting of degrees of freedom and easier preconditioning of the GMRES solver [28].

In summary, this work demonstrates that GLS4 is on par with the state-of-the-art methods for solving viscoelastic fluid flows. The method is easy to implement, because equal order polynomial interpolations can be used for all variables. The method can

further benefit from the latest developments in this field, e.g., from the logarithmic representation of the conformation tensor [34], which imposes the constraint of positive-definiteness. Other possibilities to improve the performance of GLS4 may also be considered, including adjoint of GLS or variational multiscale (VMS) [42] variant, and discontinuity capturing.

Acknowledgments

This work was supported by the National Science Foundation under award CTS-ITR-0312764 and the German Science Foundation under SFB 401, SFB 540 and SPP 1253 programs. Computational resources were provided by the Rice Terascale Cluster funded by NSF (EIA-0216467), Intel, and HewlettPackard, and the Rice Cray XD1 Research Cluster funded by NSF (CNS0421109), AMD, and Cray. Additional computing resources were provided by the RWTH Aachen Center for Computing and Communication and by the Forschungszentrum Jülich.

References

- [1] R.B. Bird, C.F. Curtiss, R.C. Armstrong, O. Hassager, Dynamics of Polymeric Liquids, vol. 2, 2nd ed., John Wiley & Sons, New York, 1987.
- [2] H.C. Öttinger, Stochastic Processes in Polymeric Fluids: Tools and Examples for Developing Simulation Algorithms, 1st ed., Springer Verlag, Berlin, 1996.
- [3] M. Grmela, P.J. Carreau, Conformation tensor rheological models, *J. Non-Newtonian Fluid Mech.* 23 (1987) 271–294.
- [4] A.N. Beris, B.J. Edwards, Thermodynamics of Flowing Systems with Internal Microstructure, 1st ed., Oxford University Press, Oxford, 1994.
- [5] R.J.J. Jongschaap, K.H. de Haas, C.A.J. Damen, A generic matrix representation of configuration tensor rheological models, *J. Rheol.* 38 (1994) 769–796.
- [6] M. Pasquali, L.E. Scriven, Theoretical modeling of microstructured liquids: a simple thermodynamic approach, *J. Non-Newtonian Fluid Mech.* 120 (2004) 101–135.
- [7] K. Feigl, M. Laso, H.C. Öttinger, CONNFESSIT approach for solving a two-dimensional viscoelastic fluid problem, *Macromolecules* 28 (1995) 3261–3274.
- [8] M.A. Hulsen, A.P.G. van Heel, B.H.A.A. van den Brule, Simulation of viscoelastic flows using Brownian configuration fields, *J. Non-Newtonian Fluid Mech.* 70 (1997) 79–101.
- [9] M. Laso, J. Ramirez, M. Picasso, Implicit micro–macro methods, *J. Non-Newtonian Fluid Mech.* 122 (2004) 215–226.
- [10] A.N. Brooks, T.J.R. Hughes, Streamline upwind/Petrov–Galerkin formulations for convection dominated flows with particular emphasis on the incompressible Navier–Stokes equations, *Comp. Meth. Appl. Mech. Eng.* 32 (1982) 199–259.
- [11] J.M. Marchal, M.J. Crochet, A new mixed finite-element for calculating viscoelastic flow, *J. Non-Newtonian Fluid Mech.* 26 (1987) 77–114.
- [12] M. Fortin, A. Fortin, A new approach for the FEM simulation of viscoelastic flows, *J. Non-Newtonian Fluid Mech.* 32 (1989) 295–310.
- [13] I. Babuška, Error-bounds for finite element method, *Numer. Math.* 16 (1971) 322–333.
- [14] F. Brezzi, On the existence, uniqueness and approximation of saddle-point problems arising from Lagrangian multipliers, *RAIRO, Modelisation Math. Anal. Numer.* 8 (1974) 129–151.
- [15] M. Fortin, R. Guénette, R. Pierre, Numerical analysis of the modified EVSS method, *Comp. Meth. Appl. Mech. Eng.* 143 (1997) 79–95.
- [16] A. Fortin, R. Guénette, R. Pierre, On the discrete EVSS method, *Comp. Meth. Appl. Mech. Eng.* 189 (2000) 121–139.
- [17] D. Rajagopalan, R.C. Armstrong, R.A. Brown, Finite element methods for calculation of steady, viscoelastic flows using constitutive equations with a Newtonian viscosity, *J. Non-Newtonian Fluid Mech.* 36 (1990) 159–192.
- [18] R. Guénette, M. Fortin, A new finite element method for computing viscoelastic flows, *J. Non-Newtonian Fluid Mech.* 60 (1995) 27–52.
- [19] M.J. Szady, T.R. Salamon, A.W. Liu, D.E. Bornside, R.C. Armstrong, R.A. Brown, A new mixed finite element method for viscoelastic flows governed by differential constitutive equations, *J. Non-Newtonian Fluid Mech.* 59 (1995) 215–243.
- [20] A.W. Liu, D.E. Bornside, R.C. Armstrong, R.A. Brown, Viscoelastic flow of polymer solutions around a periodic, linear array of cylinders—comparisons of predictions for microstructure and flow fields, *J. Non-Newtonian Fluid Mech.* 77 (1998) 153–190.
- [21] J. Sun, M.D. Smith, R.C. Armstrong, R.A. Brown, Finite element method for viscoelastic flows based on the discrete adaptive viscoelastic stress splitting and the discontinuous Galerkin method: DAVSS-G/DG, *J. Non-Newtonian Fluid Mech.* 86 (1999) 281–307.
- [22] M. Pasquali, L.E. Scriven, Free surface flows of polymer solutions with models based on the conformation tensor, *J. Non-Newtonian Fluid Mech.* 108 (2002) 363–409.
- [23] F.P.T. Baaijens, Mixed finite element methods for viscoelastic flow analysis: a review, *J. Non-Newtonian Fluid Mech.* 79 (1998) 361–385.
- [24] R.G. Owens, T.N. Phillips, Computational Rheology, 1st ed., Imperial College Press, London, 2002.
- [25] Behr, M., Stabilized finite element methods for incompressible flows with emphasis on moving boundaries and interfaces, PhD Thesis, University of Minnesota, Department of Aerospace Engineering and Mechanics, 1992.
- [26] M. Behr, L.P. Franca, T.E. Tezduyar, Stabilized finite element methods for the velocity–pressure–stress formulation of incompressible flows, *Comp. Meth. Appl. Mech. Eng.* 104 (1993) 31–48.
- [27] J. Bonvin, M. Picasso, R. Stenberg, GLS and EVSS methods for a three-field Stokes problem arising from viscoelastic flows, *Comp. Meth. Appl. Mech. Eng.* 190 (2001) 3893–3914.
- [28] M. Behr, T.E. Tezduyar, Finite element solution strategies for large-scale flow simulations, *Comp. Meth. Appl. Mech. Eng.* 112 (1994) 3–24.
- [29] M. Behr, D. Arora, O.M. Coronado, M. Pasquali, GLS-type finite element methods for viscoelastic fluid flow simulation, in: K.J. Bathe (Ed.), Proceedings of the Third MIT Conference on Computational Fluid and Solid Dynamics, Elsevier, Cambridge, MA (2005), pp. 586–589.
- [30] Y. Fan, R.I. Tanner, N. Phan-Thien, Galerkin/least-square finite-element methods for steady viscoelastic flows, *J. Non-Newtonian Fluid Mech.* 84 (1999) 233–256.
- [31] T.E. Tezduyar, S. Mittal, S.E. Ray, R. Shih, Incompressible flow computations with stabilized bilinear and linear equal-order-interpolation velocity–pressure elements, *Comp. Meth. Appl. Mech. Eng.* 95 (1992) 221–242.
- [32] R. Fattal, R. Kupferman, Constitutive laws for the matrix-logarithm of the conformation tensor, *J. Non-Newtonian Fluid Mech.* 123 (2004) 281–285.
- [33] R. Fattal, R. Kupferman, Time-dependent simulation of viscoelastic flows at high Weissenberg number using the log-conformation representation, *J. Non-Newtonian Fluid Mech.* 126 (2005) 23–37.
- [34] M.A. Hulsen, R. Fattal, R. Kupferman, Flow of viscoelastic fluids past a cylinder at high Weissenberg number: stabilized simulations using matrix logarithms, *J. Non-Newtonian Fluid Mech.* 127 (2005) 27–39.
- [35] T.J.R. Hughes, L.P. Franca, M. Balestra, A new finite element formulation for computational fluid dynamics: V. Circumventing the Babuška–Brezzi condition: a stable Petrov–Galerkin formulation of the Stokes problem accommodating equal-order interpolations, *Comp. Meth. Appl. Mech. Eng.* 59 (1986) 85–99.
- [36] T.J.R. Hughes, L.P. Franca, G.M. Hulbert, A new finite element formulation for computational fluid dynamics: VIII. The Galerkin/least-squares method for advective–diffusive equations, *Comp. Meth. Appl. Mech. Eng.* 73 (1989) 173–189.
- [37] L.P. Franca, S.L. Frey, T.J.R. Hughes, Stabilized finite element methods: I. Application to the advective–diffusive model, *Comp. Meth. Appl. Mech. Eng.* 95 (1992) 253–276.
- [38] L.P. Franca, F. Valentin, On an improved unusual stabilized finite element method for the advective–reactive–diffusive equation, *Comp. Meth. Appl. Mech. Eng.* 190 (2000) 1785–1800.

- [39] G. Hauke, A simple subgrid scale stabilized method for the advection–diffusion–reaction equation, *Comp. Meth. Appl. Mech. Eng.* 191 (2002) 2925–2947.
- [40] M.A. Alves, F.T. Pinho, P.J. Oliveira, The flow of viscoelastic fluids past a cylinder: finite-volume high-resolution methods, *J. Non-Newtonian Fluid Mech.* 97 (2001) 207–232.
- [41] X. Xie, M. Pasquali, A new, convenient way of imposing open-flow boundary conditions in two- and three-dimensional viscoelastic flows, *J. Non-Newtonian Fluid Mech.* 122 (2004) 159–176.
- [42] T.J.R. Hughes, Multiscale phenomena: Green’s functions, the Dirichlet-to-Neumann formulation, subgrid scale models, bubbles and the origins of stabilized methods, *Comp. Meth. Appl. Mech. Eng.* 127 (1995) 387–401.